Composites: Part A 145 (2021) 106367

Contents lists available at ScienceDirect

Composites Part A

journal homepage: www.elsevier.com/locate/compositesa

The influence of inter-laminar thermal contact resistance on the cooling of material during laser assisted fiber placement

Ozan Çelik [a,*], S.M. Amin Hosseini [b], Ismet Baran [b], Wouter J.B. Grouve [b], Remko Akkerman [b], Daniël M.J. Peeters [a], Julie J.E. Teuwen [a], Clemens A. Dransfeld [a]

[a] Aerospace Manufacturing Technologies, Faculty of Aerospace Engineering, Delft University of Technology, 2629HS Delft, the Netherlands
[b] Chair of Production Technology, Faculty of Engineering Technology, University of Twente, 7500AE Enschede, the Netherlands

ARTICLE INFO

Keywords:
A. Polymer-matrix composites (PMCs)
C. Process modeling
D. Microstructural analysis
E. Automated fiber placement (AFP)

ABSTRACT

The effect of thermal contact resistance (TCR) correlated to the degree of intimate contact (DIC) between the incoming tape and the substrate on the temperature history during laser-assisted fiber placement (LAFP) was investigated. A novel experimental methodology was designed to understand the effect with a non-contact method which did not influence the local consolidation quality. To assess the influence of TCR numerically, a three-dimensional optical-thermal model was developed. Experimental results indicated that, for the same tape temperature near the nip point, an increase in the compaction force resulted in a decrease in the temperature at the roller exit and the following cooling phase, in correlation with an increase in the final DIC. Also, the effect of the laser power on the final DIC was less pronounced than the compaction force. In the thermal model, when TCR at the tape-substrate interface was not considered, the temperature predictions underestimated the experimental measurements.

1. Introduction

The current production rates of lightweight composite structures are far from meeting the demand of the commercial aerospace industry. For example, the production capacity of Airbus allowed 863 aircraft to be delivered in the year 2019 [1] whereas the forecasts show that around 1900 aircraft per year will be demanded from the company over the next twenty years [2]. Automated solutions are needed to increase the production rates to the required level.

Automated Fiber Placement (AFP) is a suitable candidate for production of typical aerospace components [3]. An 8-tow AFP machine can reduce the layup time up to 20 times as compared to the conventional hand layup technique [4]. In addition to that, in situ consolidation (without a post-consolidation step in an autoclave, oven or press) is achievable with laser-assisted fiber placement (LAFP) if thermoplastic composites are used. This method has the potential for providing further reduction in cycle time, energy consumption and cost. In modern LAFP systems, a laser heat source pointed towards the nip point is used to melt the incoming tape and the substrate locally and a flexible compaction roller is used to consolidate the layers as demonstrated in Fig. 1.

During LAFP, temperature is one of the main drivers for a number of phenomena that determine the final part quality such as intimate contact development, void compaction/decompaction, crystallinity evolution, healing and residual stress development. Hence, the relationship between the process parameters and the resulting temperature history must be understood very well to predict the final quality. The majority of the research considered the nip point temperature as the most important part of the temperature history and investigated the optical-thermal phenomena that determine the temperature of the tape and substrate just before compaction. Among the high number of parameters that can be modified during the process, the effects of laser power, laser angle, spot size and placement speed on the temperature history has received notable attention so far [5–9].

The effect of the void content at the interfaces after the compaction phase on the thermal history has often been overlooked. Ideally, inter-laminar voids are eliminated by squeeze flow of the fiber-resin mixture and infiltration of the resin material through the dry fibers [10] and intimate contact is established between the incoming tape and the substrate during the compaction phase. Due to incomplete intimate contact, however, air pockets remain between the subsequent plies of the laminate. These air pockets act as insulators due to low thermal conductivity and reduce the through-thickness heat transfer as shown in

* Corresponding author.
E-mail address: ozan.celik@tudelft.nl (O. Çelik).

https://doi.org/10.1016/j.compositesa.2021.106367
Received 25 September 2020; Received in revised form 11 December 2020; Accepted 2 March 2021
Available online 19 March 2021
1359-835X/© 2021 The Author(s). Published by Elsevier Ltd. This is an open access article under the CC BY license (http://creativecommons.org/licenses/by/4.0/).

Fig. 2. This phenomenon is referred to as the inter-layer thermal contact resistance (TCR) [11]. TCR might influence the final part quality by altering the temperature history during the process.

Typically, the thermal models of the LAFP process have been built on the assumption of perfect intimate contact between the compacted tape and substrate [8,9,12,13] without experimental justification. In the work of Barasinski et al. [14], the importance of TCR for the thermal analysis of the LAFP process was mentioned. They concluded that TCR is one of the missing factors to accurately model the temperature history within the substrate. A point to note is that their experimental setup worked with a heating strategy which is different than the current LAFP systems. The tape was heated from the top instead of using a nip point heating strategy shown in Fig. 1. The highest temperature was not generated at the nip line, which resulted in a sharper difference between the temperatures of the tape and the substrate at the point of contact. Following that work, an analytical formulation of the relationship between the degree of intimate contact and TCR was presented and validated with experimental data in the work of Levy et al. [15]. It was stated that neglecting TCR would be equivalent to deviating from the actual through thickness thermal conductivity by 50%. However, the pressure used to manufacture the imperfectly bonded laminates was 1.34 kPa, which is orders of magnitude lower than the pressure levels commonly used in LAFP. Due to the aforementioned reasons, the results in both works may lead to an overestimation of the effects of TCR during LAFP.

Later on, Leon et al. [16] investigated the dependency between the fractal intimate contact model [17] and TCR numerically. The fractal dimension and material viscosity were found to have an effect on the evolution of TCR at the interface. However, no experimental work was conducted to validate the analyses. Chinesta et al. [18] and Lichtinger et al. [19] suggested finding the inter-layer TCR such that the temperature predictions of a thermal model matched the empirical temperature measurements. Such a method provided little insight on the link between the microstructure at the interfaces and the accompanying TCR. Kollmannsberger et al. [20] measured TCR for in situ consolidated laminates manufactured with and without post-consolidation and used these values to predict the temperature history with a thermal model. They compared the temperature predictions made with the experimentally obtained TCR and the equation proposed by Levy et al. [15]. Based on the results, they claimed that the equation overestimates the effect of TCR. However, the material parameters required for this equation were not measured; rather the roughness which was reported in the original publication and a constant intimate contact value of 0.75 was used without any reference to the actual degree of intimate contact of the laminate. Therefore, the theory was not related to the actual microstructure at the interfaces, which may lead to an underestimation of the effects of TCR.

To measure the effect of TCR on thermal history, thermocouples were embedded in the substrate so far [14,20]. Contact temperature measurement methods are questionable in this case, since they directly affect the intimate contact in their surroundings. Moreover, insulation material and voids around the thermocouple add more ambiguity to the obtained data. The proposed existence or non-existence of the effects of TCR in thermal history during LAFP in the literature might be a direct result of the complications introduced by adding a thermocouple to the interface. This is why this effect must be investigated with an alternative, and preferably non-contact, temperature measurement method. Thermography is such a method and it has been applied as an in situ, non-contact inspection method for AFP with thermoset prepregs. In the works of Denkena et al. [21] and Juarez and Gregory [22], a thermal camera was mounted on the rear side of the placement head. The acquired in situ temperature measurement was used to detect process-induced meso-scale defects such as gaps/overlaps, twisted/spliced tows, bridging and foreign bodies but the effect of TCR was not analyzed.

The thermal history of the newly placed tape has a significant importance since, under common processing conditions, the temperature of the material is above the melting point mostly during the initial placement [7,23]. Obviously, TCR affects the compaction and cooling phases for the newly placed tape since it requires a contact between the tape and the substrate. However, it is not possible to monitor the compaction phase of the process with current non-contact technologies.

The objective of this paper is therefore to investigate the effect of TCR (and the related degree of intimate contact) on the temperature history during the *cooling phase of the newly placed tape* considering the actual microstructure of the laminate. A novel experimental methodology and numerical model were used for the investigation. First, specimens with varying degrees of intimate contact were manufactured with a state-of-the-art LAFP setup (Section 2). During manufacturing, the temperatures before and after compaction were recorded with two long-wave infrared (LWIR) cameras. After manufacturing the samples, the degree of intimate contact at the topmost interface of the samples was measured from cross-sectional micrographs. An optical-thermal model of the process and the formulation by Levy et al. [15] were combined to calculate the temperature history for different degrees of intimate contact (Section 3). Finally, the effects of TCR were discussed combining the experimental and numerical results.

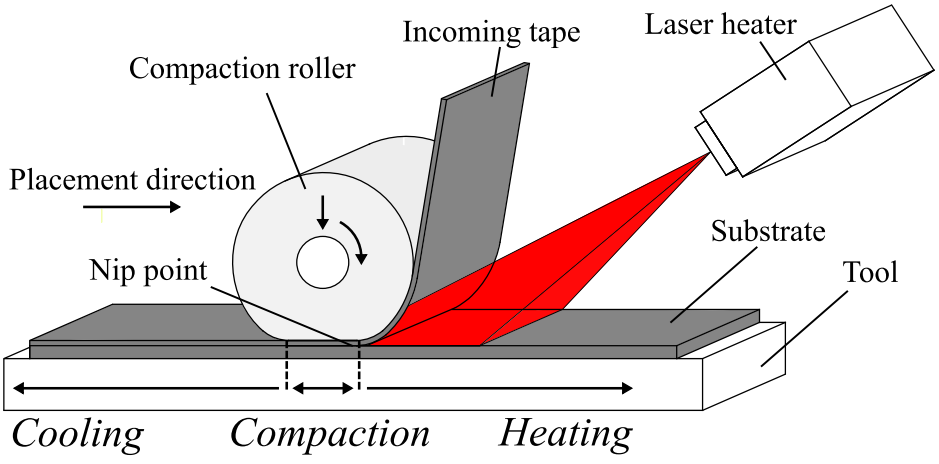

Fig. 1. Working principle of a typical LAFP system.

2. Materials and experimental methods

2.1. Fiber placement system and specimen manufacturing

The specimens were manufactured at Royal Netherlands Aerospace Center (NLR) as in a previous study [10]. A six-axis articulated robot on a linear axis provided by Coriolis was used. The machine was able to deliver eight 6.35 mm ($\frac{1}{4}$ in.)-wide tapes simultaneously with a placement speed of up to 800 mm/s. The end effector was equipped with a 6 kW Laserline LDF series diode laser system and an optic lens which created a 56 mm × 28 mm rectangular illuminated area at the 250 mm focal distance. A conformable compaction roller with 60 shore hardness and a diameter of 70 mm was installed on the machine. The roller had a coating on the outer surface which increased the contact stiffness and reduced the effects of temperature. For this study, a second thermal camera was mounted to the rear side of the machine in addition to the front thermal camera which is commonly used for process control as shown in Fig. 3.

The material used in this study was Toray Cetex TC1200 carbon fiber reinforced polyetheretherketone (CF/PEEK) tapes (fiber volume fraction 59%, melting temperature-T_m 343 °C, glass transition temperature-T_g 143 °C [24]) in 6.35 mm-wide slit form. The thickness of the prepreg was 0.15 mm. First, 1000 mm-long, $[0]_5$ substrates were placed on an aluminum tool for each specimen depositing only the odd tows (Tows 1-3-5-7 as demonstrated in Fig. 4) instead of all eight tows. This was done to reduce the laminate width so that loss of contact with the aluminum tool due to warpage was minimized. Additionally, the pressure over the width of the compaction roller was kept uniform by depositing four odd tows simultaneously. The laser power was set to 1500 W for the first layer and 1750 W for the remaining four layers. The compaction force and the placement speed were set to 500 N and 100 mm/s, respectively. These parameters were determined based on previous experience so that the substrates have low inter-laminar void content.

Following the substrate production, the sixth layer of each specimen was placed with the process parameters in Table 1. The laser power was varied so that the effects of TCR could be investigated for three different tape inlet temperatures. Throughout this paper, the term "tape inlet temperature" will be used to describe the temperature of the tape just before the nip point as it can be observed from the front thermal camera images shown in Fig. 4a. At the lowest power level, a tape inlet temperature below the melting temperature of PEEK (343 °C) was aimed for. This processing condition is not ideal for a high quality laminate since the viscosity of the CF/PEEK tape is expected to be very high, hindering the material flow at the layer interfaces. At the medium power level, the tape was kept within the processing temperature range suggested by the tape manufacturer (370–400 °C [24]). At the highest power level, a processing temperature which is highly above the melting temperature, yet below the degradation temperature (500 °C for a placement speed of 100 mm/s [7]) was aimed for. Such a tape inlet temperature was reported to result in superior laminate quality [7]. The compaction force levels were determined considering the range in which the closed loop control system can apply the desired compaction force reliably and conveniently.

2.2. Process temperature measurement

The process temperature was recorded during the placement of the sixth layer with two LWIR cameras as shown in Fig. 3. A FLIR SC325 (320 × 240 pixel-resolution, calibrated in the 200–1200 °C range to ±2 °C or ±2%) and a FLIR A35 (320 × 256 pixel-resolution, calibrated in the −40 to 550 °C range to ±5 °C or ±5%) were mounted on the front and rear sides, respectively. Examples of in situ measurements from both cameras are demonstrated in Fig. 4.

The measurements from the front camera were used to compare the effect of different laser power and compaction force values on tape inlet and substrate temperatures. Two measurement lines were placed on the tape and the substrate near the visible nip point of the fifth tow as shown in Fig. 4a. The average temperature during the steady portion of the placement course was calculated.

The rear camera was used to measure the temperature distribution along the length on the top surface of the newly placed tape at the roller exit. This was done by placing a measurement line at the centerline of the fifth tow in the thermal image as demonstrated in Fig. 4b. The length of the measurement line was determined from a calibration image in which a ruler is positioned parallel to the roller exit line (referring to Fig. 3) at 50 mm distance. The measurement line was positioned so that it extended from the roller exit to the edge of the ruler in the calibration image. The distance between the roller exit line and the calibration ruler was determined such that the measurements were performed in close vicinity to the compaction roller to avoid the effects of the macroscopic deformation, i.e. sliding of the slender laminates during placement. The average temperature distribution on the line was calculated for 100 frames where the process had reached steady state.

2.3. Intimate contact measurement

To measure the intimate contact at the topmost interface of each specimen, cross-sectional micrographs were captured and analyzed. Samples were extracted from the fifth tow of each placement trial since this tow is the closest to the center of the compaction roller in the width direction. Five 15 mm-long samples were cut along the width past the first 300 mm of the laminate, where the nip point temperature reached the steady state, as shown in Fig. 5. The samples were embedded in mounting resin, ground and polished for high quality images. A Keyence

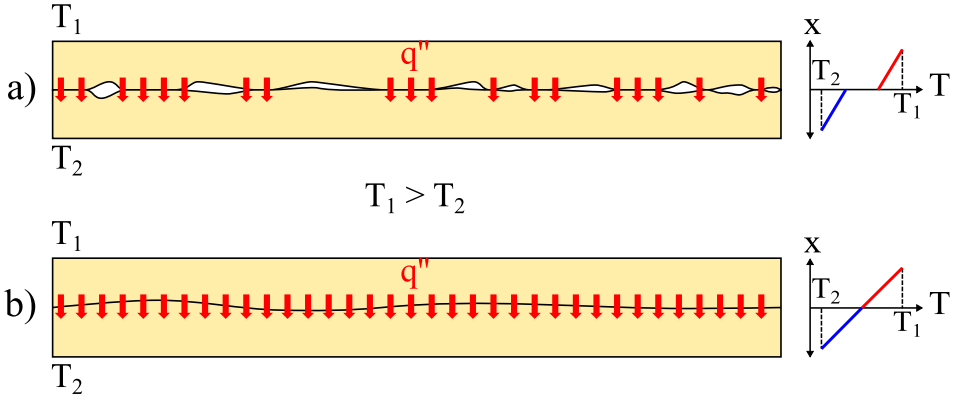

Fig. 2. Heat flux through a composite interface and example through-thickness temperature distributions for boundary temperatures T_1 and T_2 at the top and bottom surfaces, respectively. a) Incomplete intimate contact, the air pockets act as insulators and decrease the heat flux locally. b) Complete intimate contact, uniform heat flux across the whole interface.

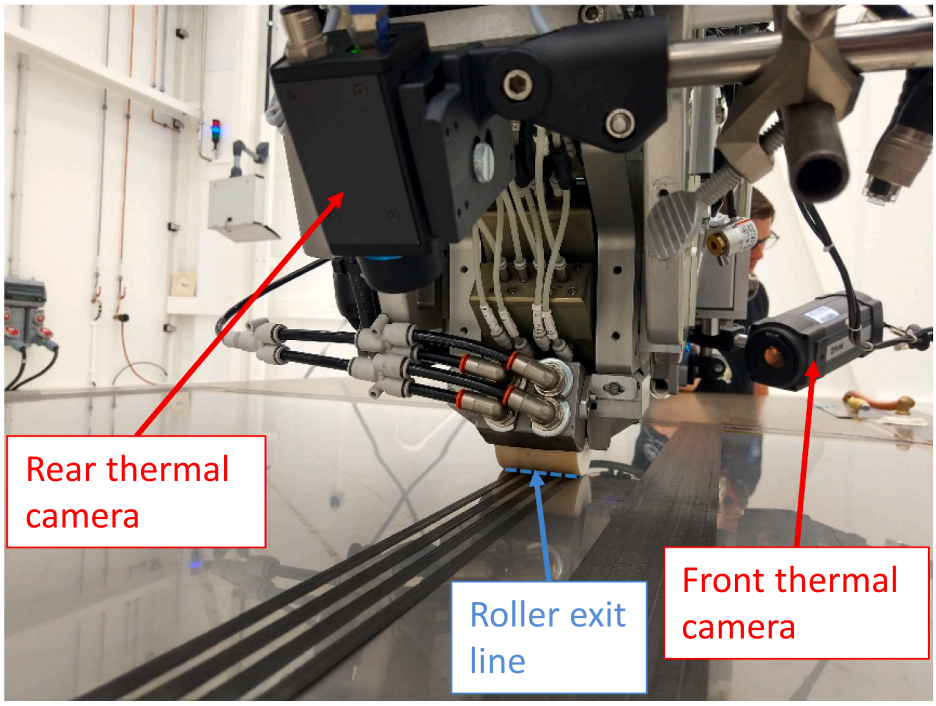

Fig. 3. Front and rear thermal cameras on the fiber placement machine to measure the tape inlet and roller exit temperatures during the process.

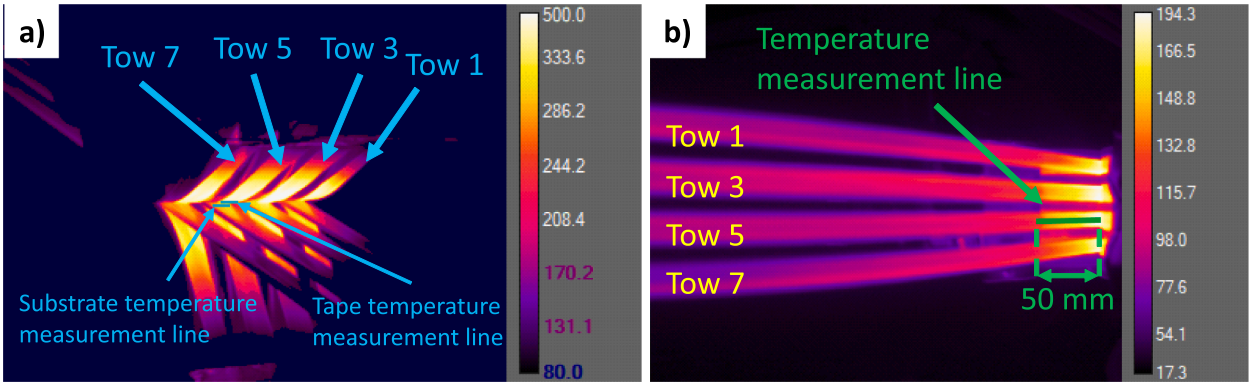

Fig. 4. Thermal images obtained from a) the front thermal camera to measure the tape inlet and substrate temperatures, b) the rear thermal camera to measure the temperature distribution at the roller exit during the process.

Table 1
Process parameters used for manufacturing the samples.

Experiment No.	Laser Power (W)	Compaction Force (N)	Placement speed (mm/s)
1	1300	100	100
2	1300	500	100
3	1300	1000	100
4	1500	100	100
5	1500	500	100
6	1500	1000	100
7	1750	100	100
8	1750	500	100
9	1750	1000	100

VK-X1000 laser microscope was used to capture the cross-sectional micrographs of the topmost interface of the laminates. The whole width of each interface was captured by stitching multiple images taken with a 50x-magnification lens to obtain high resolution images (0.55 μm/pixel).

A custom-made Matlab script was used to analyze the cross-sectional images with the methodology shown in Fig. 6. The script requires the cross-sectional image of the interface as an input (Fig. 6a). Since the topmost interface was not a straight line for most of the images, a measurement curve was defined by selecting points manually (Fig. 6b). The script allows the user to magnify the image, so the interface can be selected with high precision. This initial curve was offset by one pixel in positive and negative vertical directions to create two additional curves. This was done to ensure that the results were not affected by local features in the image without deviating too much from the bond line into the tape and substrate material. Then, a grayscale histogram was generated for each image. From this histogram, a threshold was determined with Otsu's threshold method [25] and the image was segmented such that the fiber–matrix mixture was distinguished from the voids (Fig. 6c). After the segmentation procedure, the voids and the fiber–matrix mixture at the interface can be identified by the black and white pixels, respectively (Fig. 6d). Finally, the degree of intimate contact was calculated as the ratio between the length of the white areas on the measurement curve and the total length of the measurement curve. The

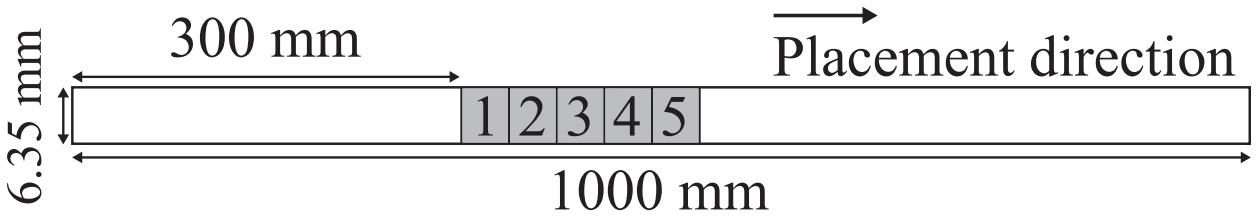

Fig. 5. Top view of the extraction locations of five samples for intimate contact investigation. The dimensions are not to scale.

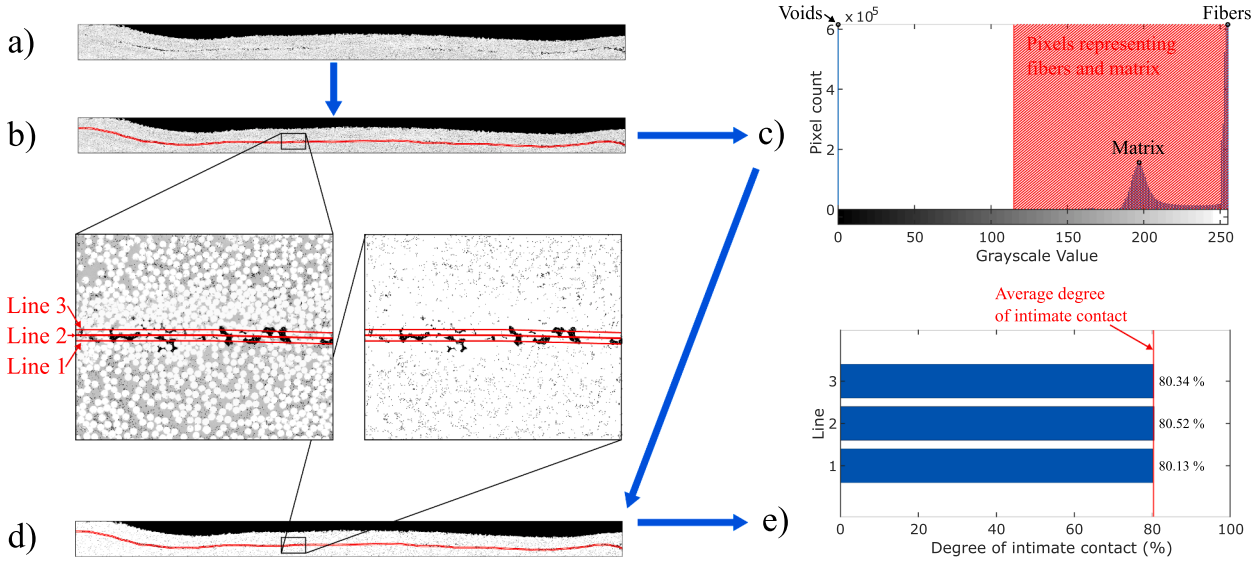

Fig. 6. Methodology for intimate contact measurement at the topmost interface from cross-sectional images. a) High resolution image of the interface. b) Definition of bond line manually (Line 2) and automatic generation of offset curves (Lines 1 and 3). The distance between the lines are not to scale. c) Segmentation of the image using the grayscale histogram and Otsu's thresholding method to distinguish the fiber–matrix mixture from the voids. d) Segmented cross-sectional image with the measurement curves. e) Calculated degree of intimate contact on each curve and the average intimate contact for the interface.

results from the three curves were averaged to obtain the final degree of intimate contact for each sample (Fig. 6e). The maximum deviation between the measured degrees of intimate contact on the three curves for an individual cross-section was 2.3%.

2.4. Analysis of variance (ANOVA)

Two-way analysis of variance (ANOVA) method was applied on the results of the temperature measurements described in Section 2.2 and intimate contact measurements described in Section 2.3 to assess the effects of the laser power and compaction force quantitatively. The Matlab built-in function *anovan* was used for this purpose [26]. The outputs of this function were p-values for each parameter investigated in Table 1. p-values smaller than 0.05 imply that the mean response of the specific parameter is different from the mean of all data within a confidence interval of 95%. The effect of such a parameter can be considered statistically significant.

3. Numerical methods

The compaction force changes a number of parameters during the LAFP process not only by altering TCR (and degree of intimate contact) via applied pressure but also changing the roller geometry. The first effect concerns the laser irradiation on the tape and substrate. As the roller deforms by increased compaction force, the location of the nip point and the shape of the incoming tape near the nip point changes. This theoretically results in a decreased shadow area and a higher temperature at the nip point [27], and hence, the roller exit. The second effect is observed during the compaction phase. An increasing compaction force extends the contact length, which causes more heat to be dissipated to the roller. This might cause a lower temperature at the roller exit [28]. Since the effects of the change in the nip point location and the contact length contradict with each other, a heat transfer model which includes an optical model and a variable roller contact length was formulated. Such a model can be used to isolate the effects of TCR on the temperature history. The following sections describe the calculation of TCR from intimate contact measurements and the temperature distribution during the process using a heat transfer model.

3.1. Thermal contact resistance calculation

To calculate the thermal contact conductance from the experimentally obtained degree of intimate contact at the interface, the equation proposed by Levy et al. [15] was used:

$$\frac{1}{C} = R = D_{ic,init} a_0 \left(\frac{1}{\lambda_{CFRP} D_{ic}^2} + \frac{1 - D_{ic}}{\lambda_{air} D_{ic}} + \frac{1}{\lambda_{CFRP}} \right) \quad (1)$$

where C is the thermal contact conductance, R is the thermal contact resistance, $D_{ic,init}$ is the initial degree of intimate contact, a_0 is the height of the rough surface layer, λ_{CFRP} is the through-thickness thermal conductivity of the composite material, D_{ic} is the degree of intimate contact at a given moment and λ_{air} is the thermal conductivity of air. This equation expresses the thermal contact conductance assuming that the interface is a thin layer of homogenized mixture of the composite and air.

During LAFP, $D_{ic,init}$ is very difficult, if not impossible, to measure with the current technology since the nip point poses extreme difficulty in positioning any kind of sensors and the consolidation takes place in a

very short time. Therefore, the initial surface profile of the tape was utilized to estimate $D_{ic,init}$ as it was done in literature [29,30] instead of the methodology proposed in Section 2.3. This methodology is not convenient to analyze the surface of an individual tape since it requires voids trapped in solidified resin at the interfaces of multiple layers to define measurement curves. $D_{ic,init}$ and a_0 were calculated from surface profiles measured from samples of unprocessed tape with an Olympus LEXT OLS3100 confocal laser scanning microscope using a × 50 lens. The resolution was 0.25 μm/pixel and the profile length was 256 μm. In total, fifteen profiles were captured. For $D_{ic}(t = 0)$, the surface profiles were approximated as a series of uniform rectangles that are schematically shown in Fig. 7. The width of the rectangles (b_0) and the surrounding gap (w_0) were found by calculating the average width of the material and gaps at different height levels within $\pm 2\sigma$ from the mean surface height, where σ designates the standard deviation. Having the dimensions of the rectangles, $D_{ic,init}$ is calculated as [29]:

$$D_{ic,init} = \frac{b_0}{b_0 + w_0} \tag{2}$$

Eq. (2) yielded an initial degree of intimate contact of 0.437 for the material used in this study. a_0 was calculated as the average standard deviation, σ, which was 12.6 μm. D_{ic} was measured for each experiment in Table 1 with the methodology described in Section 2.3. The values for λ_{CFRP} and λ_{air} were taken as 0.72 W/mK [31] and 0.0043 W/mK [32], respectively.

3.2. Heat transfer model

The transient temperature distribution during the fiber placement process was calculated with a three dimensional finite element (FE) model adapted from authors' previous work [33]. Abaqus 2017 finite element package was used to create and solve the model. The incoming tape and substrate were modeled as two stationary bodies in a Lagrangian reference frame. A moving placement head configuration was implemented, i.e. the laser illuminated area and the area where the convection coefficient was applied due to the compaction roller moved according to the placement speed. The modeling space and boundary conditions are visually demonstrated in Fig. 8.

The energy equation was solved to find the transient temperature distribution $T(t)$ within the incoming tape and substrate, with the assumption of negligible internal heat generation:

$$\rho C_p \frac{\partial T}{\partial t} = \nabla(k \nabla T) \tag{3}$$

where ρ is the density, C_p is the specific heat and k is the anisotropic thermal conductivity of the material.

The following boundary conditions were applied referring to Fig. 8. The initial temperatures of the incoming tape and substrate were defined as 20 °C. The laser irradiance, compaction roller and the nip point moved in the placement direction with the placement speed v. Until the nip point, the bottom surface of the tape and the top surface of the substrate were heated with the laser irradiance obtained from the ray tracing model proposed in [34]. This model accounts for the non-specular reflection of the laser light between the tape and substrate using a bidirectional reflectance distribution function (BRDF)-based micro-model. As schematically described in Fig. 9, several geometric parameters for the laser source, incoming tape, substrate and compaction roller are required as an input for the model. These parameters were determined from on-site measurements and Computer Aided Design (CAD) drawings of the placement head. A summary of the parameters used in the optical model is given in Table 2.

Prior to the nip point and during the compaction process (L_{c2} and L_{c1} in Fig. 8, respectively), the top surface of the tape cools down due to the contact with the compaction roller. Before and after the contact with the roller, the ambient air cools down the top surface of the tape. The heat loss to the compaction roller and the ambient air were formulated as a moving convection boundary condition:

$$k \nabla T = -h(T - T_a) \tag{4}$$

where h is the convection coefficient and T_a is the ambient temperature at the corresponding boundary. Eq. (4) was also used to express the heat loss at the bottom surface of the substrate due to the contact with the aluminum tool.

The convection coefficient (h_a) and T_a for the air were taken as 10 W/m^{2}K [35] and 20 °C, respectively. The roller and tool convection coefficients (h_r and h_t, respectively) were determined by iteratively comparing the numerical results with the temperature measurements from the top surface of the newly placed tape. This was done for the sample manufactured with a laser power of 1750 W and a compaction force of 1000 N, since the least amount of inter-laminar voids were observed in this specimen due to the high temperature and pressure. This procedure resulted in 1000 W/m^{2}K for both h_r and h_t. These values are in agreement with the values reported in the literature [31,36]. T_a was 160, 180 and 200 °C for the roller at the power levels 1300, 1500 and 1750 W, respectively (measured from the thermal images) and 20 °C for the tool.

At the tape-substrate interface, the heat transfer was modeled with a thermal contact [37]:

$$q = C(T_{tape} - T_{substrate}) \tag{5}$$

where q is the heat flux between the tape and the substrate and C is the thermal contact conductance. The value of C was updated based on the location of the moving nip point. At the regions in front of the nip point, no heat transfer was possible between the tape and the substrate. To

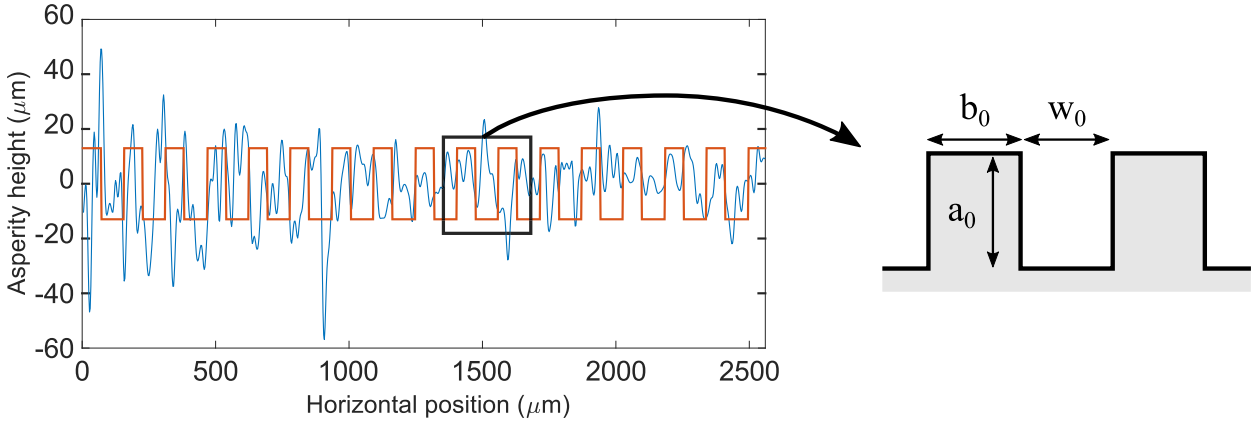

Fig. 7. Uniform rectangle idealization of the composite surface and associated geometric parameters.

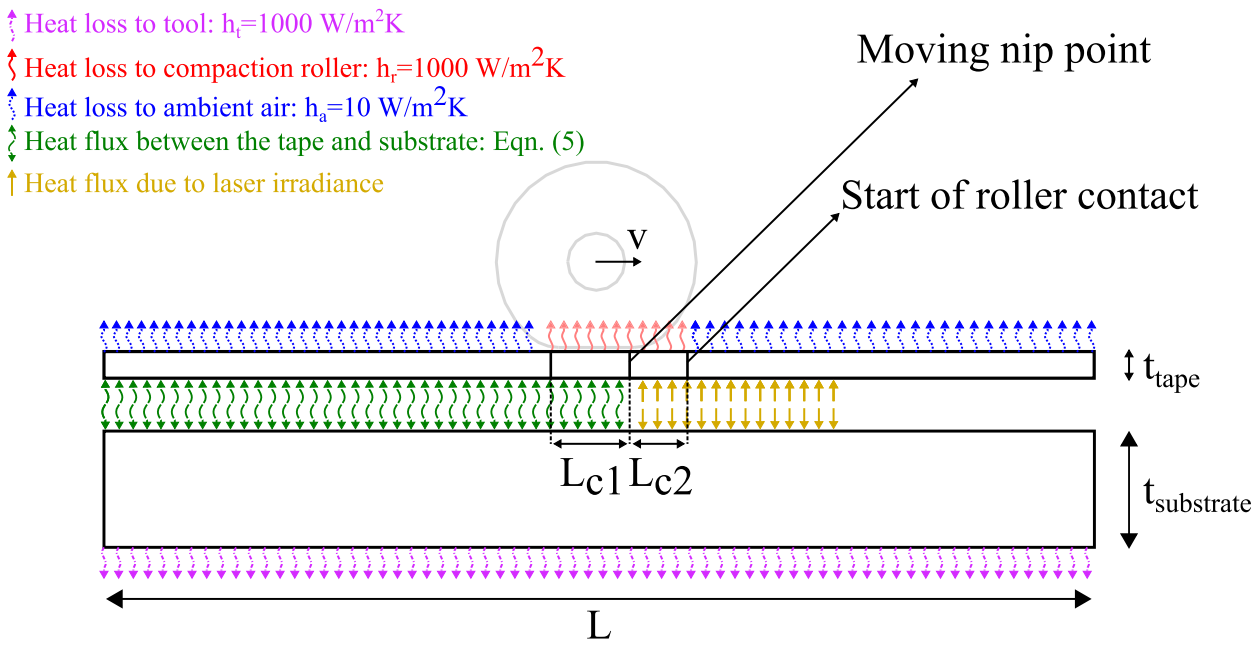

Fig. 8. Modeling space and moving boundary conditions of the FE model. h represents the applied convection coefficient. For the other parameters, please refer to Table 3.

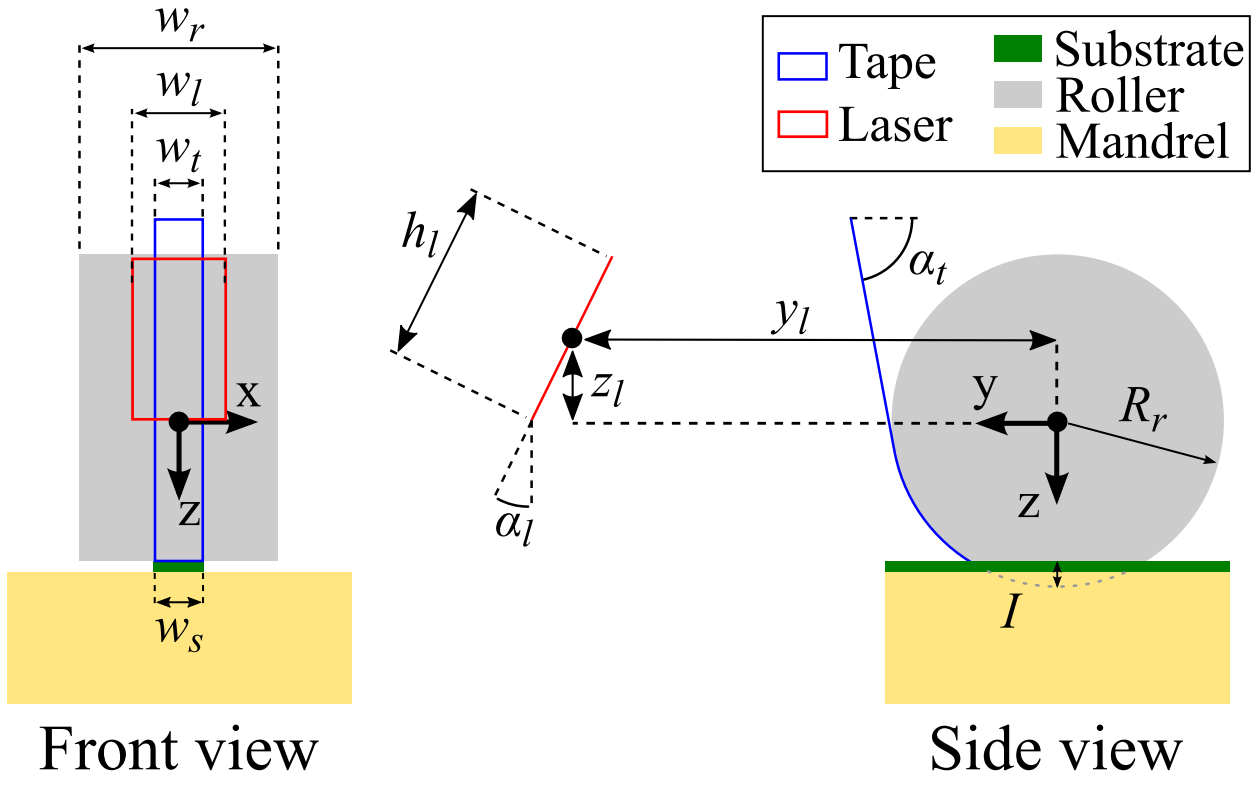

Fig. 9. Description of the optical model geometry.

impose this condition without creating numerical problems, the thermal contact conductance was set to a very low value, namely 10^{-5}W/m^{2}K. Past the nip point, the thermal contact conductance was set to the reciprocal of the value obtained from the TCR calculations explained in Section 3.1 to represent the imperfect thermal contact due to incomplete intimate contact development. A constant C was assumed immediately after the nip point. For comparison purposes, a set of simulations which represent the case of perfect intimate contact were also run by setting the thermal contact conductance to a very high value, namely 10^6W/m^{2}K.

The process settings and geometric parameters used in the model are summarized in Table 3. Thermal material properties provided in Table 4 were used for the composite material. The coordinates of the laser irradiation, area with heat loss to the compaction roller and thermal contact conductance were updated with the user subroutines DFLUX, FILM and GAPCON, respectively.

Table 2
Geometrical parameters used in the optical model.

Parameter	Description	Value
w_r	Roller width	60 mm
R_r	Roller radius	35 mm
I	Roller indentation	0.41, 0.9 and 1.47 mm (at 100, 500 and 1000 N, respectively)
w_l	Laser spot width	56 mm
h_l	Laser spot height	28 mm
y_l	Laser y-position relative to the roller center	265.3 mm
z_l	Laser z-position relative to the roller center	49.1 mm
α_l	Laser angle	18°
w_t	Tape width	6.35 mm
α_t	Tape feed angle	45°
w_s	Substrate width	6.35 mm

Table 3
The process settings and geometric parameters used in the heat transfer model.

Parameter	Symbol	Value	Unit
Placement speed	v	100	mm/s
Roller contact length in the compaction zone	L_{c1}	10.6, 15.7, 20.1 (at 100, 500 and 1000 N, respectively)	mm
Roller contact length prior to the nip point	L_{c2}	17	mm
Domain length	L	100	mm
Tape thickness	t_{tape}	0.15	mm
Tape width		6.35	mm
Substrate thickness	$t_{substrate}$	0.75	mm
Substrate width		6.35	mm

Table 4
Temperature dependent material properties of CF/PEEK [35].

Temperature	Density	Specific Heat	Thermal conductivity (W/m°C)	
(°C)	(kg/m^3°C)	(J/kg°C)	Longitudinal	Transverse
0	1601	800	3.5	0.42
50	1598	930	4.6	0.52
100	1593	1040	5.1	0.6
150	1586	1260	5.9	0.7
200	1575	1300	5.9	0.7
250	1563	1400	6.1	0.7
300	1551	1550	6.7	0.75
350	1537	1650	6.8	0.68
400	1524	1700	7	0.65

DC3D8 linear hexahedral heat transfer elements were used to mesh the tape and the tool. The tape was meshed with 10, 120 and 6 uniform elements in the thickness, length and width directions, respectively. The substrate was meshed with 120 and 6 uniform elements in the length and width directions, respectively and with 15 biased elements in the thickness direction (thickness ranging between 0.012 mm and 0.12 mm, finer near the top surface).

4. Results

4.1. Experimental process temperature

The measured tape inlet temperatures at different laser power and compaction force values are shown in Fig. 10a. Local temperature variations during LAFP have been previously observed and attributed to material inhomogeneity [38,39]. Due to differences in local fiber volume fraction, varying amounts of laser power can be absorbed at different sections of the material. The standard deviation in Fig. 10a is most likely a result of that. As the laser power increased, the tape temperature increased for all compaction force levels at an average rate of ~ 0.3 °C/W. A notable observation is that the inlet temperature was above the melting temperature of the CF/PEEK material (343 °C [24]) for the laser powers of 1500 and 1750 W, whereas it was slightly below the melting temperature for the laser power of 1300 W, as intended. A clear relation between the compaction force and the tape inlet temperature, however, was not observed. This was also reflected in the results of the ANOVA; the effect of the laser power was statistically significant ($p = 0.0002$) in contrast to the effect of the compaction force ($p = 0.2372$). Recent studies proposed that the roller deformation due to increasing compaction force has an influence on the tape temperature during the LAFP process [27]. The results in Fig. 10 show that the roller deformation did not influence the tape inlet temperature more than the experimental scatter for the experimental setup and process parameters in this study.

Fig. 10b shows the effect of laser power and compaction force on the substrate temperature. Similar to the tape, material inhomogeneity results in variation in temperature and the standard deviation for each measurement is shown. For every experiment, the average substrate temperature was below the melting temperature of PEEK. As the laser power increased, the substrate temperature increased for all compaction force levels at an average rate of ~ 0.16 °C/W. As the compaction force was increased from 100 N to 1000 N, the substrate temperature increased by 28, 23 and 15 °C for the laser powers of 1750, 1500 and 1300 W, respectively. Unlike the tape inlet temperature, a steady increase was observed for increasing compaction force levels. This result is in-line with the literature in the sense that the effect of roller deformation on the substrate temperature is more pronounced than the tape temperature [28]. The results of ANOVA shows that for the substrate

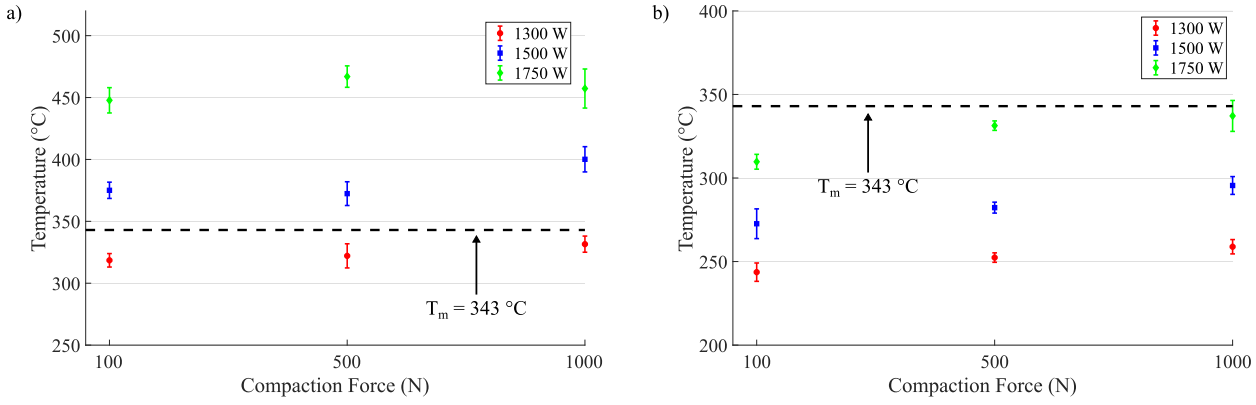

Fig. 10. a) Tape inlet and b) substrate temperatures for the fifth tow at each laser power and compaction force. Error bars represent the standard deviation. The melting temperature of PEEK is marked.

temperature, the effects of both the compaction force ($p = 0.0079$) and the laser power ($p = 0.0001$) are statistically significant.

The measured temperature histories in the cooling region at the rear side of the roller are shown in Fig. 11 with solid lines. The data was measured as a function of the distance from the roller exit line; however, it also represents the temperature history of an arbitrary location on the top surface of the tape after the roller passes over it since the placement speed is known (100 mm/s). The corresponding time is also shown in the figures. The shaded zones around the solid lines indicate the standard deviation of the 100 temperature profiles extracted with the methodology described in Section 2.2. The compaction force had an influence on the roller exit temperature for all laser power levels. An increase in the compaction force resulted in a decrease in the temperature at the roller exit. The difference between the maximum and minimum temperatures due to the various compaction forces at the roller exit was as high as 30 °C. When the compaction force was decreased to 100 N, a significant increase in temperature was observed at the roller exit compared to 500 N case (~ 20 °C), even though the tape inlet temperature was not higher and substrate temperature was even lower (Fig. 10). However, the roller exit temperature difference between the 500 N and 1000 N cases was lower (~ 10 °C). When the effect of the laser power is examined, it can be seen that the roller exit temperature increased with increasing laser power with an average rate of ~ 0.1 °C/W. The effect of the laser power on the exit temperature was lower than its effect on the tape inlet temperature. The effects of both the laser power ($p = 0.0000$) and the compaction force ($p = 0.0001$) on the roller exit temperature were statistically significant, as shown by ANOVA.

4.2. Intimate contact

Representative cross-sectional micrographs of the topmost interface of the specimens manufactured with the same laser power (1750 W) but different compaction forces (100 N and 1000 N) are shown in Fig. 12. In Fig. 12a, inter-laminar voids due to the low compaction force (100 N) can be observed. These voids are expected to reduce the through thickness heat transfer as demonstrated in Fig. 2. In contrast, high compaction force (1000 N) resulted in an almost void-free interface. The void content in the inter-laminar region was very low as shown in Fig. 12b.

The measured degree of intimate contact at the topmost interface for each parameter combination is shown in Fig. 13. The ANOVA method was used to quantify the effects of the laser power and the compaction force. The analysis showed that the laser power had a statistically insignificant effect ($p = 0.3026$) on the final degree of intimate contact whereas the effect of the compaction force was statistically significant ($p = 0.0000$). This is an interesting result since the temperature history is expected to affect intimate contact development significantly by determining the resin viscosity. Yet, the compaction force seems to drive the resulting degree of intimate contact independently of the temperature levels.

A compaction force of 100 N resulted in the lowest degree of intimate contact for all laser power levels. The degree of intimate contact increased as the compaction force was increased. The difference between the 500 N and 1000 N was smaller than the difference between the 100 N and 500 N. The reason for that can be the nonlinear relationship between the applied force and the resulting pressure under the compaction roller. As the roller is deformed further, the contact area

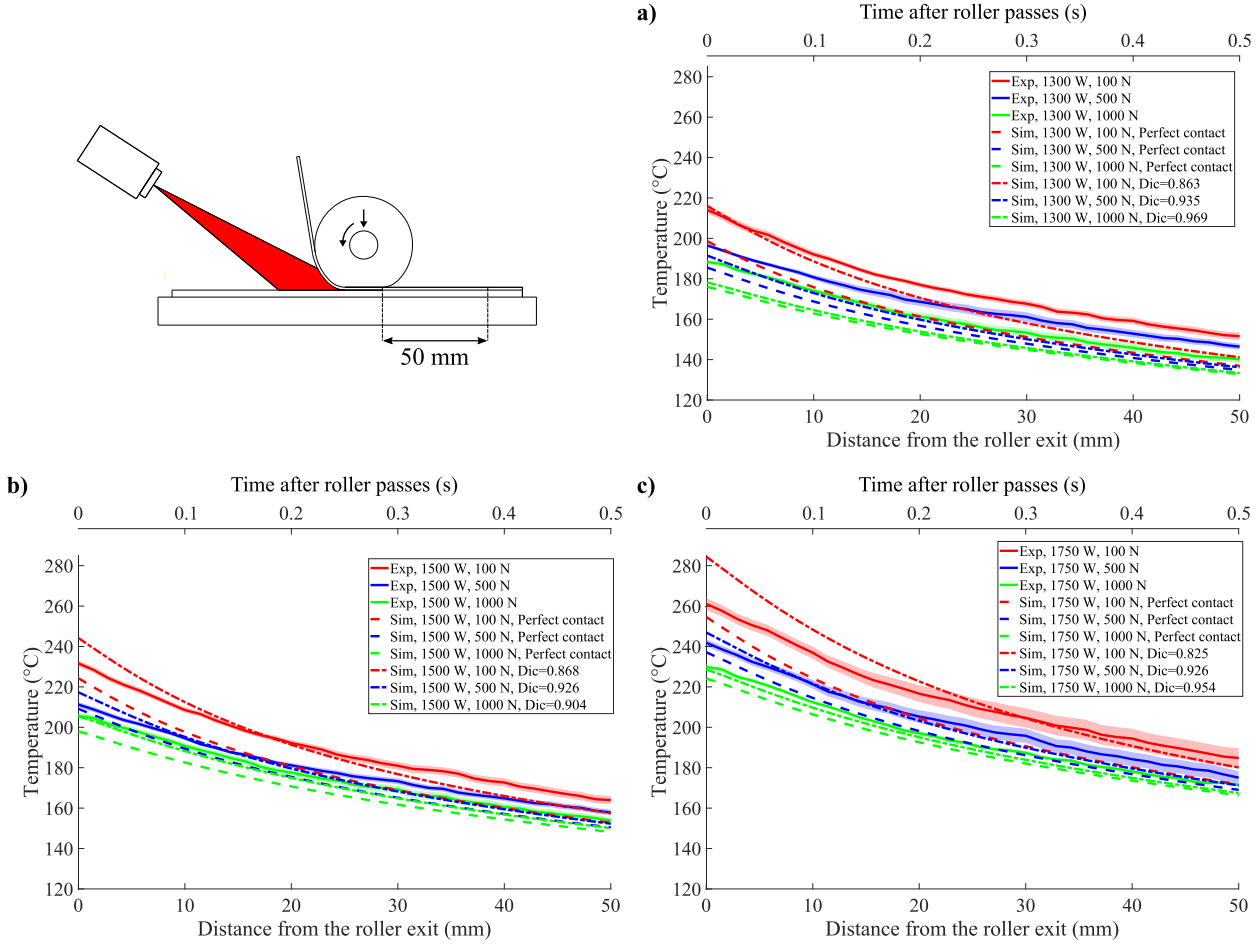

Fig. 11. Tape temperatures at the roller exit on the top surface of the fifth tow for different compaction forces and laser powers of a) 1300 W, b) 1500 W, c) 1750 W.

Fig. 12. Examples of cross-sectional micrographs of the topmost interface. a) low intimate contact (80.3%, at 1750 W and 100 N) b) high intimate contact (95.6%, at 1750 W and 1000 N).

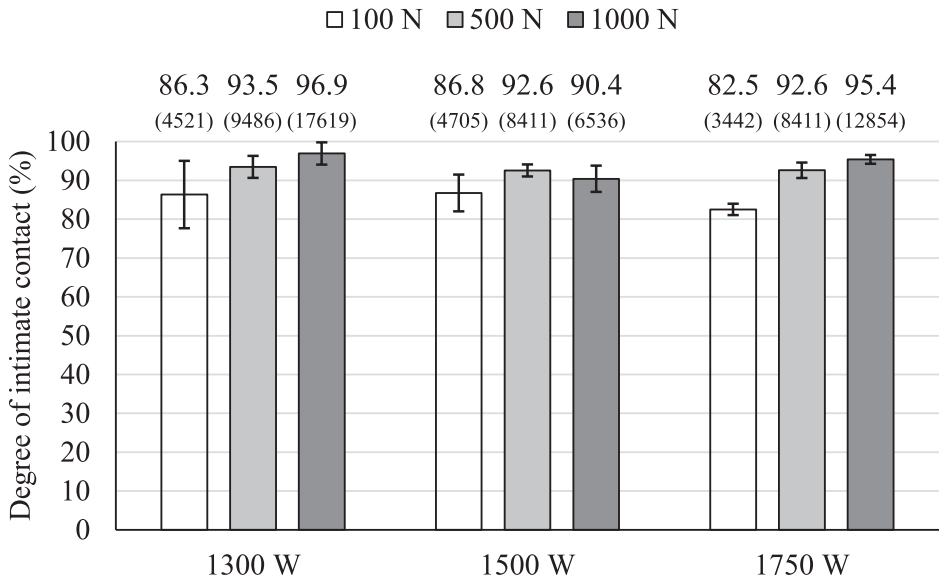

Fig. 13. Degree of intimate contact for each specimen. The horizontal axis shows the laser power and the color of each bar indicates the compaction force. The first row on top of the bars shows the average degrees of intimate contact. Error bars represent the standard deviation. Values in the parantheses show the corresponding thermal contact conductance in W/m^2K calculated using Eq. (1).

increases and limits the pressure [10]. The standard deviation increased at low compaction force for 1300 W and 1500 W. This might be a result of material scatter which could not be eliminated with the amount of pressure applied.

4.3. Calculated temperature history

4.3.1. Calculated temperature at the cooling phase

Calculated temperature histories up to 50 mm from the roller exit for each laser power and compaction force are shown in Fig. 11 with two types of dashed lines. The dash-dot lines (–·) show the temperature histories calculated with the TCR values given in Fig. 13, which were obtained from Eq. (1) for each process parameter. These temperature values will be mentioned as calculated temperature with imperfect contact (CTIC) in the upcoming discussions. In addition to those, the dashed lines (– –) present the temperature histories calculated with a very small TCR (perfect interface assumption). These will be denoted as calculated temperature with perfect contact (CTPC). As expected, CTPC resulted in a lower temperature than CTIC at any distance from the roller exit for all laser power and compaction force levels. As TCR decreased, the heat transfer from the tape to the substrate during the compaction and cooling periods became greater.

When CTIC is compared with the experimental data, it can be observed that an excellent agreement is present at the highest compaction force (1000 N) for laser powers of 1500 and 1750 W (Fig. 11b and Fig. 11c). It should be noted that the convection coefficient between the roller and the top surface of the tape was determined for the case of 1750 W and 1000 N and it was assumed that this value does not change with decreasing force. Only the change in the contact length was considered. As the compaction force was decreased at these laser power levels, the temperature calculations overshot the experimental results at the region immediately following the roller exit (approximately the first 7 mm and 20 mm for 500 N and 100 N, respectively). After this initial behavior, the calculated temperature equaled the experimental one but cooled down faster until both curves had a similar cooling trend at around 40 mm. For the lowest laser power (1300 W), the trends slightly differed as shown in Fig. 11a. For every compaction force, the temperature was underestimated with a calculated TCR for the whole distance range from the roller exit. The only exception was the temperature at the roller exit for the compaction force of 100 N, which was equal to the experimental temperature. However, CTIC cooled down faster than the experimental temperature initially as well, similar to the other laser power levels. While CTIC yielded temperature predictions comparable with the experimental data, CTPC underestimated the temperature at any distance from the roller exit for any case.

4.3.2. Calculated temperature at the compaction phase

To understand the difference between CTIC and CTPC further, calculated tape and substrate temperatures during the compaction phase of the process are presented in Fig. 14. The results are reported only for the laser power of 1750 W and compaction force of 100 N for the sake of clarity, as the combination of these parameters resulted in the least degree of intimate contact (Fig. 13) and the highest difference between CTIC and CTPC (Fig. 11). The trends did not differ for the other process parameters. The first difference can be observed at the nip point, where the bottom surface of the tape and the top surface of the substrate

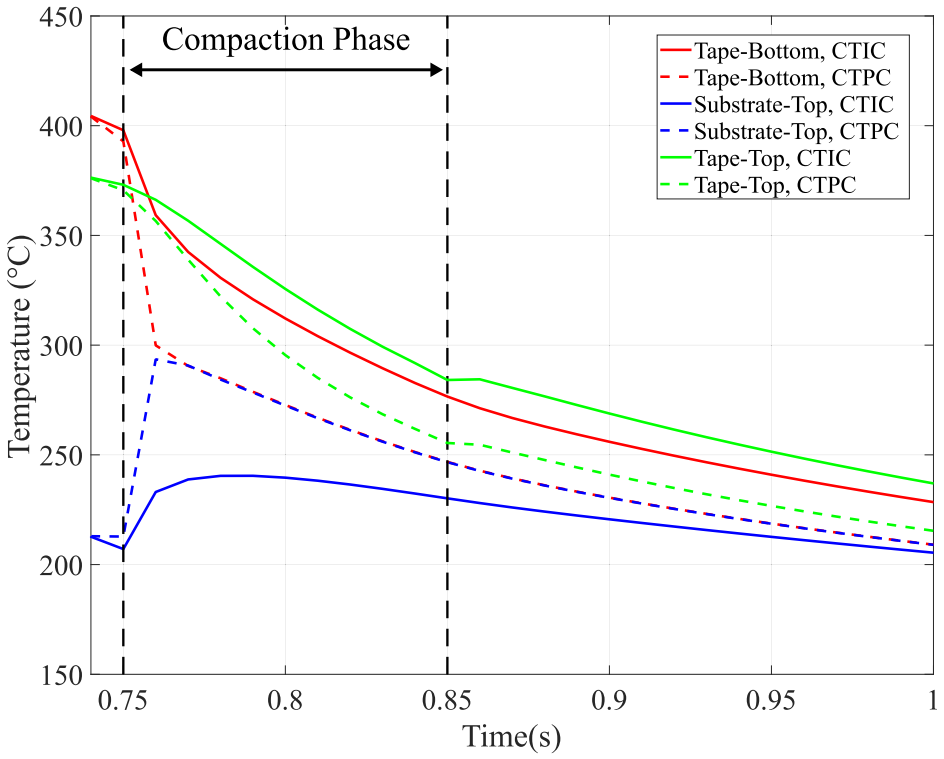

Fig. 14. Calculated temperatures for the tape and substrate during the compaction phase for the laser power of 1750 W and compaction force of 100 N.

contact each other. As expected, CTPC led to similar temperatures at the bottom surface of the tape (300 °C) and the top surface of the substrate (294 °C), which quickly equalized in the subsequent time steps. CTIC, however, resulted in a significant difference between the temperatures at the same locations of the tape (359 °C) and the substrate (233 °C). This demonstrates the effect of TCR on the heat transfer between the tape and substrate; for CTIC, cooling of the tape and heating of the substrate at the nip point were slower than CTPC. The second difference can be observed at the end of the compaction phase. The temperatures of both the bottom surface of the tape and the top surface of the substrate were 246 °C for CTPC. In the case of CTIC, these temperatures were 276 °C and 230 °C for the tape and substrate, respectively. The final difference is at the temperature of the top surface of the tape. CTIC resulted in higher temperatures at the top surface of the tape (366 °C at the nip point, 284 °C at the end of the compaction phase) than CTPC (357 °C at the nip point, 255 °C at the end of the compaction phase).

A temperature plateau can be observed at the end of the compaction zone on the top surface of the tape. The reason for that is the heat accumulation at the center of the tape in the thickness direction. During the compaction phase, a temperature gradient occurred in the thickness direction of the tape due to contact with the roller and the substrate on the opposing surfaces. As a result, in the thickness direction, the center of the tape became warmer than the surfaces. Once the roller passed, heat flowed towards the tape surfaces due to conduction within the tape. This slightly increased the temperature of the top surface momentarily, as the low convection coefficient between the ambient air and the top surface (10 W/m^2K) resulted in an almost insulated boundary. The bottom surface of the tape was not significantly affected since the main driver of cooling was the contact with the substrate with a comparatively large thermal contact conductance (>3442 Wm^2K, as shown in Fig. 13).

5. Discussion

5.1. Effect of compaction force on cooling behavior

The temperature measurements from the rear side of the compaction roller (Fig. 11) show that the compaction force has a significant influence on the temperature of the newly placed thermoplastic tape in the cooling phase of LAFP. As demonstrated in Fig. 15, it has such an importance that aft the roller exit, a tape placed with a laser power of 1300 W and a compaction force of 100 N cooled down similarly to a tape placed with a laser power of 1500 W and a compaction force of 1000 N despite the difference in energy input at the heating phase. A similar relationship holds for the laser powers of 1500 W and 1750 W as well. Since no compaction pressure is present in the cooling phase, a variation in the temperature might affect the final void content and residual stresses. In addition, the variation in the temperature due to altering compaction force has potential implications for the final degree of crystallinity of the structure, as the maximum crystallization rate of PEEK was observed between 200–280 °C [40]. Compaction force should, therefore, be considered as an integral part of any LAFP process design to control not only ply adhesion or mechanical defects such as gaps/overlaps but also the temperature history.

5.2. The role of TCR on temperature calculations

Thanks to the thermal model presented in Section 3, the effects of TCR could be separated from the other possible effects of the roller deformation induced by varying compaction force on the temperature history. When a perfect thermal contact was assumed at the interface, the model underestimated the temperature at the roller exit and the subsequent cooling period, as shown in Fig. 11. Also, numerical results presented in Fig. 14 showed that the temperature at contacting surfaces of the tape and substrate were influenced significantly during the compaction phase of the process. Therefore, in this study, it was found that TCR has a significant role in the resulting temperature history. This observation contradicts the claim that the effect of TCR is negligible for

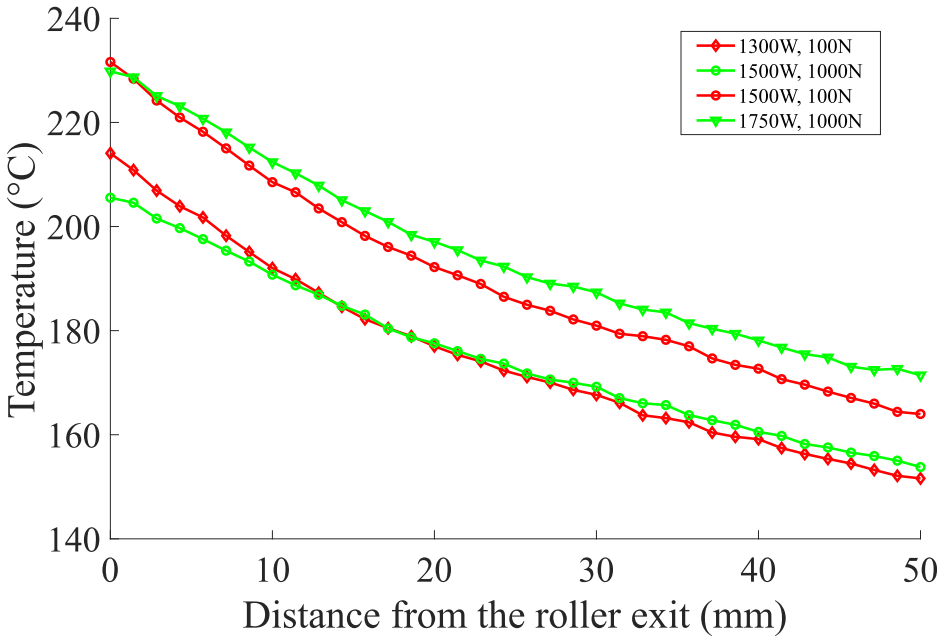

Fig. 15. Experimental temperature histories showing the effect of the compaction force on the cooling behavior observed at different power levels as a result of varying compaction force.

thermal analysis of LAFP [20]. Possibly, a laminate with a high degree of intimate contact was investigated in that study, reducing the influence of TCR on temperature history predictions. Such an effect was observed in this study as well, as demonstrated in Fig. 16. This figure shows the temperature difference between CTIC and CTPC in Fig. 11 for each experiment and the degree of intimate contact (Dic) for each curve is presented in the figure legend. The temperature difference between CTIC and CTPC was less than 10 °C at the roller exit when the degree of intimate contact was more than 90%. However, a final degree of intimate contact below 85% was reported in several works [27,41,42], meaning that TCR can not be neglected for all LAFP systems and process parameters. Moreover, as LAFP technology with in situ consolidation matures, research in the field has expanded to more complex parts such as a fuselage panel [43], variable-stiffness wingbox [44] and a pressure vessel [45]. Complex tool shapes introduce convex or concave surfaces which result in a non-uniform pressure distribution under the compaction roller [46,47], as well as transient heat flux distribution [45]. This may result in areas with insufficient intimate contact. Also, it should be noted that the results presented in this work are limited to unidirectional laminates. In a laminate consisting of layers with different orientations, intimate contact development might be lower due to the lack of fiber nesting. For such cases, the effect of TCR can be even more important.

TCR has an influence on the temperature history during the compaction and cooling phases; however, the experimental temperatures from the cooling phase were predicted with a limited accuracy when TCR was calculated with Eq. (1) using a *constant* degree of intimate

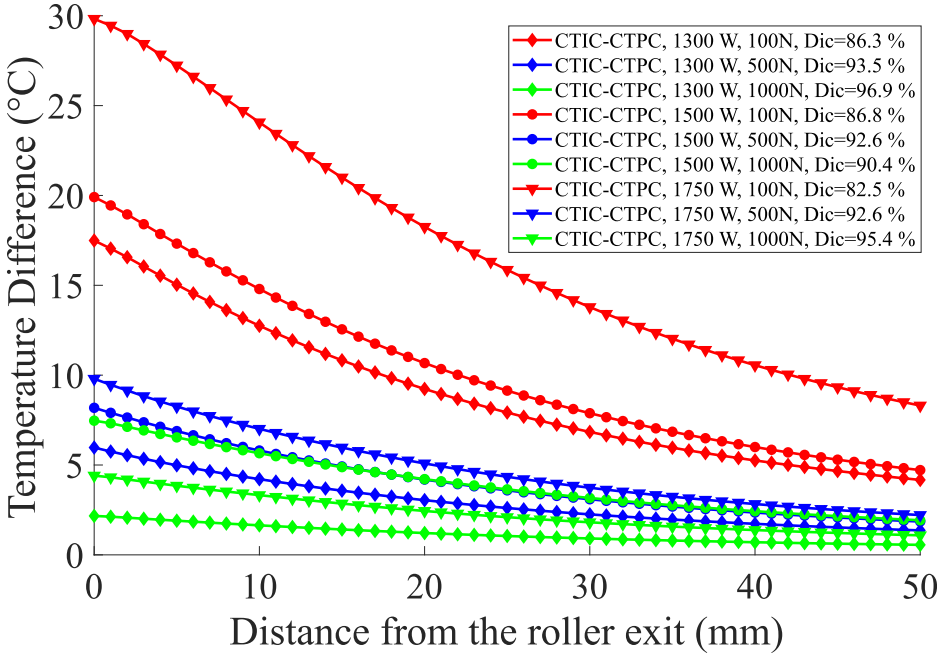

Fig. 16. The difference between the computed temperature histories using the TCR from Eq. (1) (CTIC) and a very small TCR (CTPC).

contact. The numerical results initially overshot and later underestimated the experimental results as demonstrated in Fig. 11. Such a trend suggests that TCR was not constant during the cooling phase. This behavior can be linked to void expansion after the compaction pressure was released. So far, this mechanism has been considered only for intra-laminar voids in the literature [48]. However, Fig. 12 shows that the final void content of the laminates manufactured in this study was present mostly between the topmost layer and the substrate. Based on this information, TCR evolution during the cooling phase of LAFP can be described as follows. The degree of intimate contact reached its maximum at the roller exit, causing the experimental heat flux between the tape and the substrate to be more than the calculations. Increasing heat flux caused the experimental tape temperature to be lower than the calculated temperature initially because the tape was warmer than the substrate in the experiments (shown in Fig. 10). As soon as the compaction pressure was released, the inter-laminar voids expanded and the degree of intimate contact decreased until the equilibrium between the pressure within the voids and the atmospheric pressure was reached. During the expansion of voids, the heat flux between the tape and substrate decreased and the cooling rate of the experimental temperature became lower than the calculated temperature. As a result, calculated temperatures underestimated the experimental temperatures further away from the roller exit. Additionally, in the experiments, TCR evolves during the compaction phase. It can be expected that at the nip point, the experimental TCR was higher than the numerical one, as the degree of intimate contact was low. This would result in a larger difference between the temperatures of the tape and substrate. However, as hypothesized above, the maximum degree of intimate contact was probably reached during the compaction phase. Therefore, in the experiments, the heat transfer between the tape and substrate was larger than the one calculated with the model for some duration under the compaction roller. This duration is material-specific, as the evolution of TCR is highly dependent on the surface morphology and the resin rheology [16]. Considering these phenomena, the evolution of the degree of intimate contact in the compaction and cooling phases of the process should be investigated further for a more accurate analysis of the process.

Another possible improvement to the temperature calculations is the consideration of the evolving contact between the compaction roller and the top surface of the tape. As the compaction force was increased, the contact conductance between the roller and the tape might have increased due to increasing degree of intimate contact. In this research, the effect of compaction force was implemented as a change in the contact length but the convection coefficient between the roller and the top surface of the tape was kept constant. Further research on the evolution of the thermal contact between the tape and the roller is recommended.

5.3. Origins of TCR development during LAFP

The measured degrees of intimate contact presented in Fig. 13 lead to additional interesting observations on intimate contact development, which is the source of TCR, during LAFP. Firstly, the samples manufactured with a laser power of 1300 W, which resulted in a tape inlet temperature ($\sim$ 325 °C as shown in Fig. 10) lower than the melting temperature T_m (343 °C), had the same level of degree of intimate contact as the ones manufactured with higher laser powers. This result is counter-intuitive as the semi-crystalline structure of PEEK has been considered not to allow significant softening of the polymer below T_m. In the past, several semi-crystalline polymers such as high density polyethylene (PE), polypropylene (PP), polyoxymethylene (POM), and poly (vinylidene fluoride) (PVF) were shown to be malleable between the reversible crystallization temperature (T_c)and T_m [49]. At T_c, crystal subunits are capable of moving within larger crystal units [50]. Between T_c and T_m, the mechanism for deformation was proposed to be lamellar slip and extended chain crystal formation [51]. Such a mechanism can explain intimate contact development below T_m for high performance thermoplastic composites. Recently, it was shown that CF/PEEK laminates can be thermoformed between 165–325 °C [52] and intimate contact can develop below T_m for CF/PEKK laminates during out-of-autoclave consolidation with low pressure [53]. The results in Fig. 13 confirm this point of view and show that polymer flow can take place between the T_g and T_m. Intimate contact development below T_m should be further investigated considering the reversible crystalline transition phenomenon.

Another noteworthy result is that the laser power and hence the tape inlet temperature did not have a statistically significant influence on the final degree of intimate contact, even above the melting temperature. A similar behavior was also observed for CF/PEKK tapes placed on an aluminum tool in a previous study [10]. This is unexpected since the polymer viscosity drops with increasing temperature. A possible explanation is that the interaction between the fibers in the polymer melt plays a more dominant role for intimate contact development under LAFP specific conditions such as heating without pressure, very short compaction duration and rapid cooling. It has already been shown that during the intimate contact development process, dry fibers need to be compacted [10] and this process is not primarily affected by resin viscosity. Moreover, it has been reported that the friction between the fibers has a significant part in the overall viscosity of the CF/PEEK melt and because of that an increase in temperature up to 20 °C would have little effect [54]. This study showed that intimate contact development might be insensitive to even higher temperature differences during LAFP, as the difference between the inlet temperatures was as high as 140 °C (Fig. 10).

5.4. Potential use of TCR for process inspection

In addition to understanding the influence of TCR and the mechanisms behind it for a more realistic description of the temperature history, one can exploit the phenomenon for in situ inspection of intimate contact development. With a reverse approach, the degree of intimate contact can be predicted from the measurements of the cooling behavior of the newly placed tape. This can be achieved with the optical-thermal model presented in Section 3 for flat laminates, provided that an offline database of cooling behavior is created at given LAFP process parameters for varying degrees of intimate contact (and the resulting TCR). During placement, the in situ collected data can be compared to the previously computed cooling data. The degree of intimate contact which yields the least difference between the in situ and computed data can be used as an indication of the bonding quality.

6. Conclusion

This study demonstrates the effect of the thermal contact resistance between the tape and substrate on the temperature history during the cooling phase of LAFP through dedicated experiments and numerical calculations. A novel experimental methodology was designed to understand the effect with a non-contact temperature measurement method, as contact temperature measurement methods directly influence the degree of intimate contact in their surroundings. A three-dimensional combined optical-thermal model including the thermal contact resistance between the tape and substrate was developed to assess the accuracy of the commonly preferred assumption of a perfect thermal contact in thermal analysis of the LAFP process.

Experimental results indicated that, for the same tape inlet temperature, a change in the compaction force resulted in a different temperature at the roller exit, which is in correlation with the final degree of intimate contact. As the degree of intimate contact increased, the heat transfer from the tape to substrate increased. Therefore, the tape was colder during the cooling phase. It was also observed that intimate contact can develop at temperatures below the melting temperature of the polymer.

Numerical results confirmed that neglecting thermal contact resistance at the interface causes significant underestimation of the temperature history, especially for specimens with a degree of intimate contact below 90%. Moreover, comparison between the calculated and measured temperature history led to a new hypothesis on intimate contact development during the cooling phase of LAFP. It was suggested that the expansion of voids after the pressure application should be considered not only for intra-laminar voids as commonly done in the literature but also for the inter-laminar voids.

Further research is recommended on the evolution of intimate contact (inter-laminar void expansion) during the cooling phase of LAFP. Implementation of the corresponding TCR evolution to thermal models is another path for future studies. Finally, intimate contact development below the melting temperature should be investigated for a more accurate analysis of the LAFP process.

CRediT authorship contribution statement

Ozan Çelik: Conceptualization, Methodology, Investigation, Software, Formal analysis, Visualization, Data curation, Writing - original draft, Writing - review & editing. **S.M. Amin Hosseini:** Methodology, Investigation, Software, Writing - review & editing. **Ismet Baran:** Conceptualization, Methodology, Writing - review & editing, Project administration. **Wouter J.B. Grouve:** Conceptualization, Methodology, Writing - review & editing. **Remko Akkerman:** Resources, Project administration. **Daniël M.J. Peeters:** Conceptualization, Methodology, Writing - review & editing, Supervision, Project administration. **Julie J. E. Teuwen:** Conceptualization, Methodology, Writing - review & editing, Resources, Supervision, Project administration. **Clemens A. Dransfeld:** Conceptualization, Methodology, Writing - review & editing, Resources, Supervision, Project administration.

Declaration of Competing Interest

The authors declare that they have no known competing financial interests or personal relationships that could have appeared to influence the work reported in this paper.

Acknowledgments

This work is funded by European Regional Development Fund (ERDF) within the Smart Industry Fieldlab: ACM project under Grant No. KVW-00043. The authors would also like to thank Royal Netherlands Aerospace Center (NLR), especially Chris Groenendijk and Michiel Mandemaker, for the assistance with the LAFP machine.

References

[1] Airbus. Press Release. 2020. URL https://www.airbus.com/content/dam/corporate-topics/publications/press-release/2020/02/EN-Press-Release-Airbus-FY2019-Results.pdf.
[2] Airbus. Global Market Forecast: Cities, Airports & Aircraft 2019-2038. 2019. URL https://www.airbus.com/content/dam/corporate-topics/strategy/global-market-forecast/GMF-2019-2038-Airbus-Commercial-Aircraft-book.pdf.
[3] Lukaszewicz DH, Ward C, Potter KD. The engineering aspects of automated prepreg layup: History, present and future. Compos Part B: Eng 2012;43(3):997–1009. https://doi.org/10.1016/j.compositesb.2011.12.003.
[4] Kozaczuk K. Automated fiber placement systems overview. Trans Inst Aviation 2016;245(4):52–9. https://doi.org/10.5604/05096669.1226355.
[5] Grouve WJB, Warnet LL, Rietman B, Visser HA, Akkerman R. Optimization of the tape placement process parameters for carbon-PPS composites. Compos Part A: Appl Sci Manuf 2013;50:44–53. https://doi.org/10.1016/j.compositesa.2013.03.003.
[6] Maurer D, Mitschang P. Laser-powered tape placement process – simulation and optimization. Adv Manuf: Polym Compos Sci 2015;1(3):129–37. https://doi.org/10.1080/20550340.2015.1114798.
[7] Stokes-Griffin CM, Compston P. The effect of processing temperature and placement rate on the short beam strength of carbon fibre-PEEK manufactured using a laser tape placement process. Compos Part A: Appl Sci Manuf 2015;78:274–83. https://doi.org/10.1016/j.compositesa.2015.08.008.
[8] Schaefer PM, Gierszewski D, Kollmannsberger A, Zaremba S, Drechsler K. Analysis and improved process response prediction of laser- assisted automated tape placement with PA-6/carbon tapes using Design of Experiments and numerical simulations. Compos Part A: Appl Sci Manuf 2017;96:137–46. https://doi.org/10.1016/j.compositesa.2017.02.008.
[9] Weiler T, Emonts M, Wollenburg L, Janssen H. Transient thermal analysis of laser-assisted thermoplastic tape placement at high process speeds by use of analytical solutions. J Thermoplast Compos Mater 2018;31(3):311–38. https://doi.org/10.1177/0892705717697780.
[10] Çelik O, Peeters D, Dransfeld C, Teuwen J. Intimate contact development during laser assisted fiber placement: Microstructure and effect of process parameters. Compos Part A: Appl Sci Manuf 2020;134. https://doi.org/10.1016/j.compositesa.2020.105888.
[11] Levy A, Tierney J, Heider D, Gillespie JW, Lefebure P, Lang D. Modeling of inter-layer thermal contact resistance during thermoplastic tape placement. International SAMPE Technical Conference, Baltimore, MA, USA; 2012.
[12] Hörmann P, Stelzl D, Lichtinger R, Van Nieuwenhove S, Mazón Carro G, Drechsler K. On the numerical prediction of radiative heat transfer for thermoset automated fiber placement. Compos Part A: Appl Sci Manuf 2014;67:282–8. https://doi.org/10.1016/j.compositesa.2014.08.019.
[13] Stokes-Griffin CM, Compston P. A combined optical-thermal model for near-infrared laser heating of thermoplastic composites in an automated tape placement process. Compos Part A: Appl Sci Manuf 2015;75:104–15. https://doi.org/10.1016/j.compositesa.2014.08.006.
[14] Barasinski A, Leygue A, Soccard E, Poitou A. Identification of non uniform thermal contact resistance in automated tape placement process. Int J Mater Form 2014;7(4):479–86. https://doi.org/10.1007/s12289-013-1144-9.
[15] Levy A, Heider D, Tierney J, Gillespie JW. Inter-layer thermal contact resistance evolution with the degree of intimate contact in the processing of thermoplastic composite laminates. J Compos Mater 2014;48(4):491–503. https://doi.org/10.1177/0021998313476318.
[16] Leon A, Barasinski A, Chinesta F. Microstructural analysis of pre-impreganted tapes consolidation. Int J Mater Form 2017;10(3):369–78. https://doi.org/10.1007/s12289-016-1285-8.
[17] Yang F, Pitchumani R. A fractal Cantor set based description of interlaminar contact evolution during thermoplastic composites processing. J Mater Sci 2001;36(19):4661–71. https://doi.org/10.1023/A:1017950215945.
[18] Chinesta F, Leygue A, Bognet B, Ghnatios C, Poulhaon F, Bordeu F, et al. First steps towards an advanced simulation of composites manufacturing by automated tape placement. Int J Mater Form 2014;7(1):81–92. https://doi.org/10.1007/s12289-012-1112-9.
[19] Lichtinger R, Hörmann P, Stelzl D, Hinterhölzl R. The effects of heat input on adjacent paths during Automated Fibre Placement. Compos Part A: Appl Sci Manuf 2015;68:387–97. https://doi.org/10.1016/j.compositesa.2014.10.004.
[20] Kollmannsberger A, Lichtinger R, Hohenester F, Ebel C, Drechsler K. Numerical analysis of the temperature profile during the laser-assisted automated fiber placement of CFRP tapes with thermoplastic matrix. J Thermoplast Compos Mater 2018;31(12):1563–86. https://doi.org/10.1177/0892705717738304.
[21] Denkena B, Schmidt C, Völtzer K, Hocke T. Thermographic online monitoring system for Automated Fiber Placement processes. Compos Part B: Eng 2016;97:239–43. https://doi.org/10.1016/j.compositesb.2016.04.076.
[22] Juarez PD, Gregory ED. In situ thermal inspection of automated fiber placement manufacturing. AIP Conf Proc 2019;2102:120002. https://doi.org/10.1063/1.5099847.
[23] Di Francesco M, Valverde MA, Ward C, Giddings PF, Dell' Anno G, Potter K. Influence of layup speed on the quality of thermoplastic preforms manufactured by laser- assisted automated fibre placement. ECCM17 - 17th European Conference on Composite Materials, Munich, Germany; 2016.
[24] Composites TA. TenCate Cetex TC1200 PEEK Resin System Product Data Sheet; 2017.
[25] Otsu N. A threshold selection method from gray-level histograms. IEEE Trans Syst, Man Cybernet 1979;9(1):62–6. https://doi.org/10.1109/TSMC.1979.4310076.
[26] The MathWorks Inc. MATLAB and Statistics Toolbox Release 2017b. 2017.
[27] Kok T. On the consolidation quality in laser assisted fiber placement: the role of the heating phase. Phd thesis. University of Twente; 2018. https://doi.org/10.3990/1.9789036546065.
[28] Hosseini SMA, Baran I, van Drongelen M, Akkerman R. On the temperature evolution during continuous laser-assisted tape winding of multiple C/PEEK layers: The effect of roller deformation. Int J Material Forming 2020. https://doi.org/10.1007/s12289-020-01568-7.
[29] Lee WI, Springer GS. A model of the manufacturing process of thermoplastic matrix composites. J Compos Mater 1987;21(11):1017–55. https://doi.org/10.1177/002199838702101103.
[30] Tierney J, Gillespie JW. Modeling of in situ strength development for the thermoplastic composite tow placement process. J Compos Mater 2006;40(16):1487–506. https://doi.org/10.1177/0021998306060162.
[31] Ghasemi Nejhad MN, Cope R, Güceri SI. Thermal analysis of in-situ thermoplastic composite tape laying. J Thermoplast Compos Mater 1991;4(1):20–45. https://doi.org/10.1177/089270579100400102.
[32] Ageorges C, Ye L, Mai YW, Hou M. Characteristics of resistance welding of lap shear coupons. Part I: Heat transfer. Compos Part A: Appl Sci Manuf 1998;29(8):899–909. https://doi.org/10.1016/S1359-835X(98)00022-0.
[33] Çelik O, Shroff S, Teuwen JJE, Bergsma OK, Benedictus R. A 3-D finite element model for thermal analysis of laser assisted fiber placement. Southampton, UK: SAMPE Europe; 2018.

[34] Reichardt J, Baran I, Akkerman R. New analytical and numerical optical model for the laser assisted tape winding process. Compos Part A: Appl Sci Manuf 2018;107:647–56. https://doi.org/10.1016/j.compositesa.2018.01.029.
[35] Cogswell FN. Thermoplastic aromatic polymer composites: a study of the structure, processing, and properties of carbon fibre reinforced polyetheretherketone and related materials. Butterworth-Heinemann; 1992. https://doi.org/10.1016/B978-0-7506-1086-5.50002-1.
[36] Kim HJ, Kim SK, Lee WI. A study on heat transfer during thermoplastic composite tape lay-up process. Exp Thermal Fluid Sci 1996;13(4):408–18. https://doi.org/10.1016/S0894-1777(96)00095-7.
[37] Dassault Systèmes. ABAQUS 2017 Documentation. 2017.
[38] Zaami A, Schäkel M, Baran I, Bor TC, Janssen H, Akkerman R. Temperature variation during continuous laser-assisted adjacent hoop winding of type-IV pressure vessels: An experimental analysis. J Compos Mater 2019. https://doi.org/10.1177/0021998319884101.
[39] Stokes-Griffin CM, Kollmannsberger A, Compston P, Drechsler K. The effect of processing temperature on wedge peel strength of CF/PA 6 laminates manufactured in a laser tape placement process. Compos Part A: Appl Sci Manuf 2019;121:84–91. https://doi.org/10.1016/j.compositesa.2019.02.011.
[40] Tardif X, Pignon B, Boyard N, Schmelzer JW, Sobotka V, Delaunay D, et al. Experimental study of crystallization of PolyEtherEtherKetone (PEEK) over a large temperature range using a nano-calorimeter. Polym Testing 2014;36:10–9. https://doi.org/10.1016/j.polymertesting.2014.03.013.
[41] Stokes-Griffin CM, Compston P. Investigation of sub-melt temperature bonding of carbon-fibre/PEEK in an automated laser tape placement process. Compos Part A: Appl Sci Manuf 2016;84:17–25. https://doi.org/10.1016/j.compositesa.2015.12.019.
[42] Di Francesco M, Giddings PF, Scott M, Goodman E, Dell'Anno G, Potter K. Influence of laser power density on the meso-structure of thermoplastic composite preforms manufactured by Automated Fibre Placement. SAMPE Long Beach 2016;53:1689–99. https://doi.org/10.1017/CBO9781107415324.004.
[43] Rodriguez-Lence F, Martin MI, Fernandez Horcajo K. In-situ consolidation of integrated thermoplastic fuselage panels: The future in structural comercial aerocomposites. In: ECCM 2018–18th European Conference on Composite Materials. ISBN 9781510896932; 2018.
[44] Oliveri V, Zucco G, Peeters D, Clancy G, Telford R, Rouhi M, et al. Design, manufacture and test of an in-situ consolidated thermoplastic variable-stiffness wingbox. AIAA Journal 2019;57(4):1671–83. https://doi.org/10.2514/1.J057758.
[45] Hosseini SMA, Schäkel M, Baran I, Janssen H, van Drongelen M, Akkerman R. A new global kinematic-optical-thermal process model for laser-assisted tape winding with an application to helical-wound pressure vessel. Mater Des 2020;193:108854. https://doi.org/10.1016/j.matdes.2020.108854.
[46] Lichtinger R, Lacalle J, Hinterhölzl R, Beier U, Drechsler K. Simulation and experimental validation of gaps and bridging in the automated fiber placement process. Sci Eng Compos Mater 2015;22(2):131–48. https://doi.org/10.1515/secm-2013-0158.
[47] Peeters D, Clancy G, Oliveri V, O'Higgins R, Jones D, Weaver PM. Concurrent design and manufacture of a thermoplastic composite stiffener. Compos Struct 2019;212:271–80. https://doi.org/10.1016/j.compstruct.2019.01.033.
[48] Pitchumani R, Ranganathan S, Don RC, Gillespie JW, Lamontia MA. Analysis of transport phenomena governing interfacial bonding and void dynamics during thermoplastic tow-placement. Int J Heat Mass Transf 1996;39(9):1883–97. https://doi.org/10.1016/0017-9310(95)00271-5.
[49] Aharoni SM, Sibilia JP. Crystalline transitions and the solid-state extrusion of polymers. J Appl Polym Sci 1979;23(1):133–40. https://doi.org/10.1002/app.1979.070230112.
[50] Aharoni SM, Sibilia JP. Extrudability of crystalline polymers. Polym Eng Sci. 1979;19(6):450–5.
[51] Bigg DM. Mechanical property enhancement of semicrystalline polymers–A review. Polymer Eng Sci 1988;28(13):830–41. https://doi.org/10.1002/pen.760281303.
[52] Zheng B, Gao X, Li M, Deng T, Huang Z, Zhou H, et al. Formability and failure mechanisms of woven CF/PEEK composite sheet in solid-state thermoforming. Polymers 2019;11(6). https://doi.org/10.3390/polym11060966.
[53] Saffar F, Sonnenfeld C, Beauchêne P, Park CH. In-situ monitoring of the out-of-autoclave consolidation of carbon/ poly-ether-ketone-ketone prepreg laminate. Front Mater 2020;7(June):1–12. https://doi.org/10.3389/fmats.2020.00195.
[54] Deignan A, Stanley WF, McCarthy MA. Insights into wide variations in carbon fibre/polyetheretherketone rheology data under automated tape placement processing conditions. J Compos Mater 2017. https://doi.org/10.1177/0021998317740733.